

Article

Correlating Pure Component Properties with MOSCED Solubility Parameters: Enthalpy of Vaporization and Vapor Pressure

Nick H. Wong , Pratik Dhakal , Sydnee N. Roese and Andrew S. Paluch * 

Department of Chemical, Paper, and Biomedical Engineering, Miami University, Oxford, OH 45056, USA

* Correspondence: paluchas@miamioh.edu or MOSCED@MiamiOH.edu; Tel.: +1-(513)-529-0784

Abstract: Tools to predict vapor–liquid phase equilibria are indispensable for the conceptualization and design of separation processes. Modified separation of cohesive energy density (MOSCED) is a solubility-parameter-based method parameterized to make accurate predictions of the limiting activity coefficient. As a solubility-parameter-based method, MOSCED can not only make quantitative predictions, but can shed light on the underlying intermolecular interactions. In the present study, we demonstrated the ability of MOSCED to correlate the enthalpy of vaporization and vapor pressure at a specific temperature using multiple linear regression. With this addition, MOSCED is able to predict vapor–liquid phase equilibria in the absence of reference data. This was demonstrated for the prediction of the Henry’s constant and solvation free energy of organic solutes in water, which was found to be superior to mod-UNIFAC. In addition to being able to make phase equilibrium predictions, the ability to correlate the enthalpy of vaporization and vapor pressure offers the opportunity to include additional properties in the regression of the MOSCED parameters. Given this success, we additionally attempted to correlate a wide range of physical properties using a similar expression. While, in some cases, the results were reasonable, they were inferior to the correlations of the enthalpy of vaporization and vapor pressure. Future efforts will be needed to improve the correlations.

Keywords: solubility parameter; phase equilibrium; Henry’s constant; solvation free energy; enthalpy of vaporization; vapor pressure



Citation: Wong, N.H.; Dhakal, P.; Roese, S.N.; Paluch, A.S. Correlating Pure Component Properties with MOSCED Solubility Parameters: Enthalpy of Vaporization and Vapor Pressure. *ChemEngineering* **2023**, *7*, 25. <https://doi.org/10.3390/chemengineering7020025>

Academic Editor: Roumiana Petrova Stateva

Received: 11 January 2023

Revised: 16 February 2023

Accepted: 9 March 2023

Published: 18 March 2023



Copyright: © 2023 by the authors. Licensee MDPI, Basel, Switzerland. This article is an open access article distributed under the terms and conditions of the Creative Commons Attribution (CC BY) license (<https://creativecommons.org/licenses/by/4.0/>).

1. Introduction

Methods to predict phase equilibria are crucial for the design of industrial separation processes, which typically constitute 40–70% of both the capital and operating cost of a chemical plant. Separation processes are non-spontaneous processes requiring an external “separating agent”, typically either energy or a solvent, which make them expensive [1]. Here, we considered vapor–liquid separation processes, which include distillation, absorption, and stripping. Distillation alone constitutes approximately 90–95% of the separation processes used in practice and, in the United States, accounts for approximately 11% of all in-plant energy consumed [2,3].

Solubility-parameter-based methods have long been utilized for early-stage process conceptualization and design applications as a result of their ability to both predict the phase equilibrium and shed light on the underlying intermolecular interactions [4–12]. When using these methods to compute limiting activity coefficients, we decompose the log limiting activity coefficient into the sum of a combinatorial (COMB) and residual (RES) contribution, where the COMB contribution results from size and shape dissimilarities between the components in the system and the RES contribution results from intermolecular interactions. The COMB contribution may be computed using available athermal solution theories, such as the Flory–Huggins or Flory–Huggins–Staverman–Guggenheim equations [4,13,14].

The earliest solubility parameter method to predict the RES contribution was Hildebrand and Scatchard's "Regular Solution Theory" (RST). However, RST is limited in that it can only predict positive contributions, as well as being limited to modeling dispersion interactions [4,5]. Solubility parameter methods have been greatly improved by splitting the solubility parameter into a sum of contributions [5,11]. Perhaps the most-well-known of these methods is the Hansen solubility parameter (HSP), which accounts for dispersion, polar, and hydrogen bonding interactions [6]. This results in an expression of the RES contribution of the limiting activity coefficient of the form:

$$\ln \gamma_2^{\text{RES},\infty} = \frac{v_2}{RT} \left[(\lambda_2 - \lambda_1)^2 + (\tau_2 - \tau_1)^2 + (\alpha_2\beta_2 - \alpha_1\beta_1)^2 \right] \quad (1)$$

where $\gamma_2^{\text{RES},\infty}$ is the RES contribution of the limiting activity coefficient of Component 2, R is the molar gas constant, T is the absolute temperature, v_2 is the pure component molar volume of Component 2, λ_i is the pure component solubility parameter of component i , which accounts for the dispersion interactions, τ_i is the pure component solubility parameter of component i , which accounts for the polar interactions, and $\alpha_i\beta_i$ is the pure component solubility parameter of component i , which accounts for hydrogen bonding (or association), where $i = \{1, 2\}$. Within the hydrogen bonding term, $\alpha_i\beta_i$ corresponds to self-association, where α_i accounts for the hydrogen bond donating ability and β_i accounts for the hydrogen bond accepting ability of component i . However, HSP is still limited in that it can only predict positive RES contributions. Tijssen et al. [12] overcame this limitation by splitting the hydrogen bonding term, resulting in [12]

$$\ln \gamma_2^{\text{RES},\infty} = \frac{v_2}{RT} \left[(\lambda_2 - \lambda_1)^2 + (\tau_2 - \tau_1)^2 + 2(\alpha_2 - \alpha_1)(\beta_2 - \beta_1) \right] \quad (2)$$

This expression forms the basis of modified separation of cohesive energy density (MOSCED), which we utilized here [15–24]. It should be noted that this splitting has recently been suggested to improve the accuracy of the HSP [10].

The limiting activity coefficient accounts for solute–solvent and solvent–solvent interactions and corresponds to the maximum deviation from the ideal solution behavior. Moreover, the limiting activity can be used to predict a wide range of phase equilibria for early-stage design applications [25]. For example, Henry's constant for Component 2 in 1 ($\mathcal{H}_{2,1}$) may be computed as [24]

$$\ln \mathcal{H}_{2,1}(T, P) = \ln \gamma_2^\infty(T, P) + \ln P_2^{\text{sat}}(T) \quad (3)$$

and the fundamental solvation free energy of Component 2 in 1 ($\Delta G_{2,1}^{\text{solv}}$) [24]:

$$\frac{1}{RT} \Delta G_{2,1}^{\text{solv}}(T, P) = \ln \gamma_2^\infty(T, P) + \ln \frac{v_1(T, P) P_2^{\text{sat}}(T)}{RT} \quad (4)$$

where T and P are the temperature and pressure, respectively, P_2^{sat} is the vapor pressure of pure Component 2, R is the molar gas constant, and v_1 is the molar volume of Component 1, where we made the standard assumptions that the vapor phase is an ideal gas and the Poynting correction is negligible such that the pure component fugacity is equal to the pure component vapor pressure. Likewise, for the case of isothermal vapor–liquid equilibrium, it can be shown that, for a mono-azeotropic system, for a system to exhibit a minimum boiling azeotrope [26,27]:

$$\gamma_2^\infty(T) > \frac{P_1^{\text{sat}}(T)}{P_2^{\text{sat}}(T)} > \frac{1}{\gamma_1^\infty(T)} \quad (5)$$

and for a system to exhibit a maximum boiling azeotrope [26,27]:

$$\gamma_2^\infty(T) < \frac{P_1^{\text{sat}}(T)}{P_2^{\text{sat}}(T)} < \frac{1}{\gamma_1^\infty(T)} \quad (6)$$

where P_1^{sat} is the vapor pressure of pure Component 1 and Component 1 corresponds to the most-volatile component ($P_1^{\text{sat}} > P_2^{\text{sat}}$). It is additionally possible to use limiting activity coefficients to parameterize a binary interaction excess Gibbs free energy model, which may then be used to extrapolate to finite concentrations. For the case of Wilson's equation, we have [4,24,28]

$$\begin{aligned}\ln \gamma_1 &= -\ln(x_1 + \Lambda_{12}x_2) + x_2 \left(\frac{\Lambda_{12}}{x_1 + \Lambda_{12}x_2} - \frac{\Lambda_{21}}{\Lambda_{21}x_1 + x_2} \right) \\ \ln \gamma_2 &= -\ln(x_2 + \Lambda_{21}x_1) - x_1 \left(\frac{\Lambda_{12}}{x_1 + \Lambda_{12}x_2} - \frac{\Lambda_{21}}{\Lambda_{21}x_1 + x_2} \right)\end{aligned}\quad (7)$$

where Λ_{12} and Λ_{21} are adjustable parameters, which may be related to the binary (intermolecular) interaction parameters (BIPs) of the system (a_{12} and a_{21}):

$$\begin{aligned}\Lambda_{12} &= \frac{v_2}{v_1} \exp \left[-\frac{a_{12}}{RT} \right] \\ \Lambda_{21} &= \frac{v_1}{v_2} \exp \left[-\frac{a_{21}}{RT} \right]\end{aligned}\quad (8)$$

At infinite dilution, Equation (7) reduces to

$$\begin{aligned}\ln \gamma_1^\infty &= -\ln(\Lambda_{12}) + 1 - \Lambda_{21} \\ \ln \gamma_2^\infty &= -\ln(\Lambda_{21}) + 1 - \Lambda_{12}\end{aligned}\quad (9)$$

which can be used to solve for parameters Λ_{12} and Λ_{21} . This may, in turn, be used to model vapor–liquid equilibrium, where

$$\begin{aligned}x_1\gamma_1P_1^{\text{sat}} &= y_1P \\ x_2\gamma_2P_2^{\text{sat}} &= y_2P\end{aligned}\quad (10)$$

where y_1 and y_2 are the vapor phase mole fraction of Components 1 and 2, respectively, and recall $x_1 + x_2 = 1$ and $y_1 + y_2 = 1$.

Be that as it may, Equations (3)–(6) and (10) all require knowledge of the pure component vapor pressure. While the vapor pressure is available for a wide range of fluids, the ability to predict vapor pressure using MOSCED parameters would be of great value for early-stage process conceptualization and design applications. It has previously been shown that MOSCED parameters may be used to correlate the enthalpy of vaporization [29,30]. Given the relationship between the enthalpy of vaporization and log vapor pressure via the Clapeyron equation, we hypothesized that the correlation of the vapor pressure should also be possible. Likewise, Abraham solute descriptors have been used to correlate a wide range of thermophysical properties, including the enthalpy of vaporization and vapor pressure [31–33]. Since MOSCED parameters correspond to physical interactions, we expected that it should likewise be possible to use them as descriptors to correlate and predict vapor pressure.

Recently in 2005, MOSCED was subject to a “revision”, wherein the literature was surveyed and the parameters were regressed for 130 organic solvents, water, 2-room-temperature ionic liquids (ILs), and 5 non-condensable gases using experimental limiting activity coefficients [20]; this was recently expanded to an additional 33 1-*n*-alkyl-3-methylimidazolium-based ILs [34,35]. The further expansion of MOSCED is limited by the availability of experimental limiting activity coefficients. The ability to use MOSCED to correlate pure component properties could be of additional value in that it would allow one to incorporate additional data into the regression of new parameters. This has been demonstrated previously for MOSCED with the use of the enthalpy of vaporization [36]. Additionally, recent efforts have been made to predict MOSCED parameters devoid of experimental data. This includes the use of molecular simulation and electronic structure calculation to generate reference data [30,36–39] and traditional group contribution meth-

ods [29,36]. The present study is complementary to this work, wherein it presents the opportunity to predict phase equilibrium for early stage process conceptualization and design applications.

Know that many excellent methods exist to predict pure component properties from molecular structures. For example, the group contribution method of Gani and co-workers can be used to predict a wide range of pure component properties [40,41]. This includes the critical temperature, pressure, and acentric factor, which, in turn, could be used to predict vapor pressure using a cubic equation of state. Likewise, Gharagheizi et al. [42] recently developed a group contribution/machine learning method to predict vapor pressure directly. As mentioned earlier, Abraham solute descriptors have been used to correlate a wide range of thermophysical properties including vapor pressure [32]. The goal of the present study was to assess the ability to use MOSCED parameters to correlate and predict pure component properties, specifically the enthalpy of vaporization and vapor pressure. This would allow for the prediction of phase equilibrium using only MOSCED parameters for early-stage process conceptualization and design applications and, additionally, provides the opportunity to incorporate additional data into the parameterization of MOSCED. Moreover, in general, the ability to predict pure component properties and to provide molecular-level insight via the solubility parameter would be of great utility.

In the present study, we demonstrated the ability to successfully correlate the enthalpy of vaporization and vapor pressure at a specific temperature. Furthermore, we demonstrated the ability to use the predicted enthalpy of vaporization to extrapolate the predicted vapor pressure to additional temperatures. This was applied to predict $\mathcal{H}_{2,1}$ and $\Delta G_{2,1}^{\text{soliv}}$. We also summarize our results, wherein we attempted to correlate additional pure component properties, but with limited success.

2. Method

2.1. Theory

Using MOSCED, the log limiting activity coefficient of Component 2 (solute) in Component 1 (solvent), $\ln \gamma_2^\infty$, is computed as [15,20]

$$\begin{aligned} \ln \gamma_2^\infty &= \ln \gamma_2^{\text{COMB},\infty} + \ln \gamma_2^{\text{RES},\infty} \\ \ln \gamma_2^{\text{COMB},\infty} &= \ln \left(\frac{v_2}{v_1} \right)^{aa_2} + 1 - \left(\frac{v_2}{v_1} \right)^{aa_2} \\ \ln \gamma_2^{\text{RES},\infty} &= \frac{v_2}{RT} \left[(\lambda_1 - \lambda_2)^2 + \frac{q_1^2 q_2^2 (\tau_1^{(T)} - \tau_2^{(T)})^2}{\psi_1} + \frac{(\alpha_1^{(T)} - \alpha_2^{(T)})(\beta_1^{(T)} - \beta_2^{(T)})}{\xi_1} \right] \\ aa_2 &= 0.953 - 0.002314 \left[(\tau_2^{(T)})^2 + \alpha_2^{(T)} \beta_2^{(T)} \right] \\ \alpha_i^{(T)} &= \alpha_i \left(\frac{293 \text{ K}}{T} \right)^{0.8}, \beta_i^{(T)} = \beta_i \left(\frac{293 \text{ K}}{T} \right)^{0.8}, \tau_i^{(T)} = \tau_i \left(\frac{293 \text{ K}}{T} \right)^{0.4}, \text{ where } i = \{1 \text{ or } 2\} \\ \psi_1 &= \text{POL} + 0.002629 \alpha_1^{(T)} \beta_1^{(T)} \\ \xi_1 &= 0.68(\text{POL} - 1) + \left[3.4 - 2.4 \exp(-0.002687(\alpha_1 \beta_1)^{1.5}) \right]^{(293 \text{ K}/T)^2} \\ \text{POL} &= q_1^4 \left[1.15 - 1.15 \exp(-0.002337(\tau_1^{(T)})^3) \right] + 1 \end{aligned} \quad (11)$$

where $\ln \gamma_2^{\text{COMB},\infty}$, $\ln \gamma_2^{\text{RES},\infty}$ correspond to the combinatorial and residual contribution to $\ln \gamma_2^\infty$, respectively, v_i is the (liquid) molar volume, λ_i , τ_i , α_i , and β_i are the solubility parameters due to dispersion, polarity, and hydrogen bond acidity and basicity, respectively, and the induction parameter, q_i , reflects the ability of the non-polar part of a molecule to interact with a polar part, where $i = \{1, 2\}$. The terms ψ_1 and ξ_1 are (solvent-dependent) asymmetry terms; these terms are not adjustable, but are a function of the solvent solubility parameters. The asymmetry terms are important for the accuracy of MOSCED and are intended to account for the fact that descriptors are solute solubility parameters,

and the interactions of a component as a solute at infinite dilution are different than a component as a solvent (in the pure component limit) [43]. The superscript (T) is used to indicate temperature-dependent parameters, where the temperature dependence is computed using the empirical correlations provided in Equation (11). As suggested by the equations, MOSCED adopts a reference temperature of 293 K (20 °C). The COMB term is modeled using a modified athermal Flory/Huggins equation, where aa_2 is an empirical (solute-dependent) term to modify the size dissimilarity for polar and hydrogen bonding interactions. The term aa_2 is not adjustable, but is a function of the solubility parameters of the solute. For all cases, $aa_2 \leq 0.953$, which reduces the effective size dissimilarity and magnitude of the combinatorial contribution, with the value smaller for polar and associating compounds. An equivalent expression for the limiting activity coefficient for Component 1 in 2 ($\ln \gamma_1^\infty$) can be written by switching the subscript indices in Equation (11).

MOSCED is based on the theory that the cohesive energy may be separated into individual contributions (due to specific intermolecular interactions), which are additive. MOSCED is a “modified” separation in that empirical asymmetry terms are introduced, which improve the accuracy of the model, in addition to the splitting of the association term. Both modifications are physically, but not theoretically justified. We, therefore, expected that we can relate the MOSCED parameters (partial solubility parameters) to the total cohesive energy (ΔU^{coh}). Following the work of [12], which, like MOSCED, splits the association parameter, we expected an expression of the form:

$$\frac{\Delta U^{\text{coh}}}{RT} = \frac{v}{RT} (a_1 \lambda^2 + a_2 \tau^2 + a_3 \alpha \beta) \quad (12)$$

where a_1 , a_2 , and a_3 are constants that have been introduced to account for the empiricism introduced by MOSCED. In Equation (12), the cohesive energy is written as the sum of the contributions due to the dispersion ($v\lambda^2$), polar ($v\tau^2$), and association ($v\alpha\beta$) interactions. Assuming the vapor phase is an ideal gas and that the molar volume of the vapor phase is much greater than the liquid phase, the cohesive energy may be related to the enthalpy of vaporization (ΔH^{vap}) as

$$\frac{\Delta H^{\text{vap}}}{RT} = \frac{\Delta U^{\text{coh}} + RT}{RT} = \frac{\Delta U^{\text{coh}}}{RT} + 1 = a_0 + \frac{v}{RT} (a_1 \lambda^2 + a_2 \tau^2 + a_3 \alpha \beta) \quad (13)$$

where, in theory, $a_0 = 1$ is a constant. In this light, we view a_0 as being equal to a reference value of $\Delta H^{\text{vap}}/(RT)$, our property of interest, and the term $v/(RT)(a_1 \lambda^2 + a_2 \tau^2 + a_3 \alpha \beta)$ as the deviation between the reference and actual value. Previously, it has been shown that using $a_0 = 1$ and taking a_1 to be either adjustable or $a_1 = 1$, Equation (13) can be used to accurately correlate ΔH^{vap} at 20 °C [29,30]. In this expression, the term $\alpha\beta$ corresponds to self-association interactions. Here, we also considered the following modified expression:

$$\frac{\Delta H^{\text{vap}}}{RT} = a_0 + \frac{v}{RT} (a_1 \lambda^2 + a_2 \tau^2 + a_3 \alpha \beta + a_4 \alpha \alpha + a_5 \beta \beta) \quad (14)$$

where the self-association interaction term ($\alpha\beta$) is complemented with separate terms accounting for the hydrogen bond donating ($\alpha\alpha$) and accepting ($\beta\beta$) strength. In addition to correlating ΔH^{vap} at 20 °C, we also investigated the ability to correlate ΔH^{vap} at 0 and 40 °C. With the ability to predict ΔH^{vap} at three temperatures for a given compound, one could extrapolate and interpolate to other temperatures, for example using a modified Watson’s equation of the form:

$$H^{\text{vap}} = A \left(1 - \frac{T}{B}\right)^n \quad (15)$$

where A , B , and n are all adjustable constants [44,45]. Note that, while in our previous work, we correlated ΔH^{vap} in units of kJ/mol, here we divided through by the term RT to form dimensionless terms.

Furthermore, via the Clapeyron equation, $\ln P^{\text{sat}} \propto \Delta H^{\text{vap}}$. We, therefore, investigated the ability to correlate $\ln P^{\text{sat}}$ at a given temperature as

$$\ln P^{\text{sat}} = a_0 + \frac{v}{RT} (a_1 \lambda^2 + a_2 \tau^2 + a_3 \alpha \beta) \quad (16)$$

and

$$\ln P^{\text{sat}} = a_0 + \frac{v}{RT} (a_1 \lambda^2 + a_2 \tau^2 + a_3 \alpha \beta + a_4 \alpha \alpha + a_5 \beta \beta) \quad (17)$$

We again considered the case of 0, 20, and 40 °C. The intention was again that the ability to predict $\ln P^{\text{sat}}$ at three temperatures for a given compound would allow one to extrapolate and interpolate to other temperatures, for example using an Antoine equation of the form:

$$\ln P^{\text{sat}} = A - \frac{B}{T + C} \quad (18)$$

where A , B , and C are all adjustable constants. Within Equations (16) and (17), the second term on the right-hand side is dimensionless, and we took $a_0 = \ln P_0^{\text{sat}}$ to be equal to a reference value of $\ln P^{\text{sat}}$, such that $\ln P^{\text{sat}} - a_0 = \ln P^{\text{sat}} / P_0^{\text{sat}}$ is dimensionless.

2.2. Data Compilation and Regression

In the most-recent MOSCED revision in 2005, the parameters were regressed for 130 organic solvents and water using experimental limiting activity coefficients [20]. Here, we considered only the organic solvents. Additionally we excluded acetic acid because of the difficulties in measuring ΔH^{vap} and $\ln P^{\text{sat}}$ experimentally; monocarboxylic acids are known to associate strongly in the vapor phase with the measured values of ΔH^{vap} and $\ln P^{\text{sat}}$ corresponding to a vapor phase consisting of a mixture of monomers and dimers [46]. In Equation (12), we assumed the vapor phase is an ideal gas, so the monomer value is needed. Reference values of ΔH^{vap} and $\ln P^{\text{sat}}$ at 0, 20, and 40 °C were sourced from *Yaws' Handbook of Thermodynamic and Physical Properties of Chemical Compounds* [45] for as many of the organic solvents as possible at each temperature. The compiled reference data are provided in the Supporting Information accompanying the electronic version of this manuscript.

For Equations (13), (14), (16) and (17), the parameters were regressed using multiple linear regression with MATLAB [47]. The problem was formulated and solved using linear algebra and required the use of only basic matrix operations [48]. To quantify the goodness of fit, we subsequently computed the Pearson correlation coefficient (R^2), the root-mean-squared error (RMS), and the average absolute percent error (AAPE).

To further assess the accuracy with which we can predict $\ln P^{\text{sat}}$ and the sensitivity of the resulting phase equilibrium calculations, we predicted $\mathcal{H}_{2,1}$ and $\Delta G_{2,1}^{\text{soln}}$ for all possible organic compounds in water using Equations (3) and (4) for which MOSCED parameters existed and reference data were available. The reference values for $\mathcal{H}_{2,1}$ were taken from *Yaws' Handbook of Properties for Aqueous Systems* [49], and the reference values for $\Delta G_{2,1}^{\text{soln}}$ were taken from the the FreeSolv database [50–52]. These are the same reference sets we used previously to assess MOSCED [34].

3. Results and Discussion

3.1. Regression

A summary of the regressed model parameters and goodness of fit is provided in Table 1 for the use of Equations (13) and (16) to correlate $\ln P^{\text{sat}}$ and $\Delta H^{\text{vap}} / (RT)$, respectively. In general, the correlation takes the form:

$$X = a_0 + \frac{v}{RT} (a_1 \lambda^2 + a_2 \tau^2 + a_3 \alpha \beta) \quad (19)$$

where X is the property of interest and a_0 can be considered the reference value of property X .

Table 1. Summary of the regressed model parameters using Equations (13) and (16) along with the Pearson correlation coefficient (R^2), the root-mean-squared error (RMS), and the average absolute percent error (AAPE) to assess the goodness of fit, where N corresponds to the number of organic compounds included in the fit. In the correlations, P^{sat} is in units of bar and ΔH^{vap} corresponds to $\Delta H^{\text{vap}}/(RT)$, which is dimensionless. The temperature indicates the temperature at which the regression was performed.

Property	a_0	a_1	a_2	a_3	R^2	RMS	AAPE (%)	N
$\ln P^{\text{sat}}$ (0 °C)	4.94	−0.63	−1.65	−1.48	0.93	0.88	18.14	102
$\ln P^{\text{sat}}$ (20 °C)	5.14	−0.61	−1.61	−1.38	0.94	0.80	90.14	113
$\ln P^{\text{sat}}$ (40 °C)	5.34	−0.59	−1.59	−1.32	0.93	0.74	40.79	116
ΔH^{vap} (0 °C)	3.38	0.94	2.20	2.92	0.91	1.65	6.86	95
ΔH^{vap} (20 °C)	2.76	0.93	2.27	2.88	0.92	1.46	6.59	107
ΔH^{vap} (40 °C)	2.04	0.93	2.35	2.81	0.93	1.33	6.67	113

In general, we found the correlations to be very good; in all cases, $R^2 > 0.9$. Considering first the case of $\Delta H^{\text{vap}}/(RT)$, we found that a_0 is not equal to 1, as suggested by Equations (12) and (13). Comparing to our previous work [29], there, we set $a_0 = a_1 = 1$ at 20 °C and obtained $R^2 = 0.933$, $a_2 = 2.8373$, and $a_3 = 3.1152$ for 81 organic compounds (which also excluded acetic acid). Likewise, correlating the cohesive energy density, the work of Gnap and Elliott [30] suggested that $a_0 = a_1 = 1$, $a_2 = 2.5$, and $a_3 = 3$, where acetic acid was also excluded. We found that here, the value of a_1 was close to 1, as well as $a_3 > a_2$ with similar values.

While this previous work suggested that we could achieve a similar accuracy of $\Delta H^{\text{vap}}/(RT)$ with $a_0 = a_1 = 1$, here, we made the parameters adjustable in an attempt to generalize the ability of MOSCED to correlate arbitrary physical properties comparable to a traditional group contribution method (see, for example, the work of Gani and co-workers [40,41]). In this light, the terms λ^2 (dispersion), τ^2 (polar), and $\alpha\beta$ (self-association) correspond to physical descriptors. For $\Delta H^{\text{vap}}/(RT)$, we found that physical interactions increase the value of $\Delta H^{\text{vap}}/(RT)$ with respect to the reference value, with the effect of dispersion less than polar interactions and polar slightly less than self-association interactions. This agrees with physical intuition.

Considering $\ln P^{\text{sat}}$, we again found that the correlation was very good. Compared to the reference value, we found that the physical interactions decreased the value of $\ln P^{\text{sat}}$, where, here, the effect of dispersion was less than self-association interactions and self-association slightly less than polar interactions.

Next, a summary of the regressed model parameters and goodness of fit is provided in Table 2 for the use of Equations (14) and (17) to correlate $\ln P^{\text{sat}}$ and $\Delta H^{\text{vap}}/(RT)$, respectively. In general, the correlation takes the form:

$$X = a_0 + \frac{v}{RT} \left(a_1 \lambda^2 + a_2 \tau^2 + a_3 \alpha\beta + a_4 \alpha\alpha + a_5 \beta\beta \right) \quad (20)$$

where we added two additional terms corresponding to the hydrogen bond donating ($\alpha\alpha$) and accepting ($\beta\beta$) ability.

Table 2. Summary of the regressed model parameters using Equations (14) and (17) along with the Pearson correlation coefficient (R^2), the root-mean-squared error (RMS), and the average absolute percent error (AAPE) to assess the goodness of fit, where N corresponds to the number of organic compounds included in the fit. In the correlations, P^{sat} is in units of bar, and ΔH^{vap} corresponds to $\Delta H^{\text{vap}}/(RT)$, which is dimensionless. The temperature indicates the temperature at which the regression was performed.

Property	a_0	a_1	a_2	a_3	a_4	a_5	R^2	RMS	AAPE (%)	N
$\ln P^{\text{sat}}$ (0 °C)	4.94	-0.63	-1.64	-1.59	0.11	0.00	0.93	0.87	18.25	102
$\ln P^{\text{sat}}$ (20 °C)	5.13	-0.61	-1.64	-1.34	-0.04	0.01	0.94	0.80	100.47	113
$\ln P^{\text{sat}}$ (40 °C)	5.30	-0.58	-1.56	-1.26	-0.03	-0.01	0.93	0.74	40.35	116
ΔH^{vap} (0 °C)	3.40	0.94	2.18	3.11	-0.20	0.00	0.91	1.65	6.85	95
ΔH^{vap} (20 °C)	2.78	0.93	2.28	2.82	0.04	0.00	0.92	1.45	6.54	107
ΔH^{vap} (40 °C)	2.07	0.90	2.34	2.74	0.04	0.01	0.93	1.32	6.62	113

We again found that we were able to well correlate $\ln P^{\text{sat}}$ and $\Delta H^{\text{vap}}/(RT)$. We found that the parameters changed little, with the values of a_4 and a_5 close to 0, further demonstrating that the additional terms had little effect. Nonetheless, moving forward in this work, we focused on the use of Equation (20). While the two additional parameters had little effect, we still had a model with only six adjustable parameters that may readily be regressed.

The ability of Equation (17) to correlate $\ln P^{\text{sat}}$ is illustrated in Figures 1 and 2, a parity and residual plot, respectively. In Figure 1, we see that the values of $\ln P^{\text{sat}}$ were well correlated. In Figure 2, the error appears random. However, it does appear that the smaller the value of $\ln P^{\text{sat}}$, the larger the deviation between the calculated and reference value was. As noted earlier, the effect of intermolecular interactions was to decrease the value of $\ln P^{\text{sat}}$ as compared to the reference value. Therefore, the larger the deviation from the reference value, the larger the observed error was.

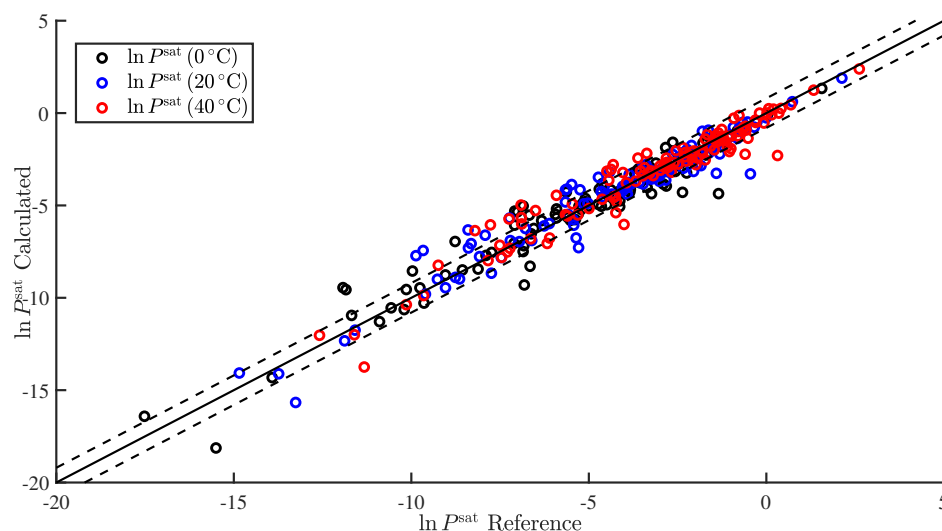


Figure 1. Parity plot of $\ln P^{\text{sat}}$ calculated using Equation (17) at 0, 20, and 40 °C, as indicated, versus the reference values. P^{sat} is in units of bar. The solid line corresponds to the $y = x$ line, and the dashed lines correspond to plus or minus the root-mean-squared error (RMS) at 20 °C and are drawn as a reference.

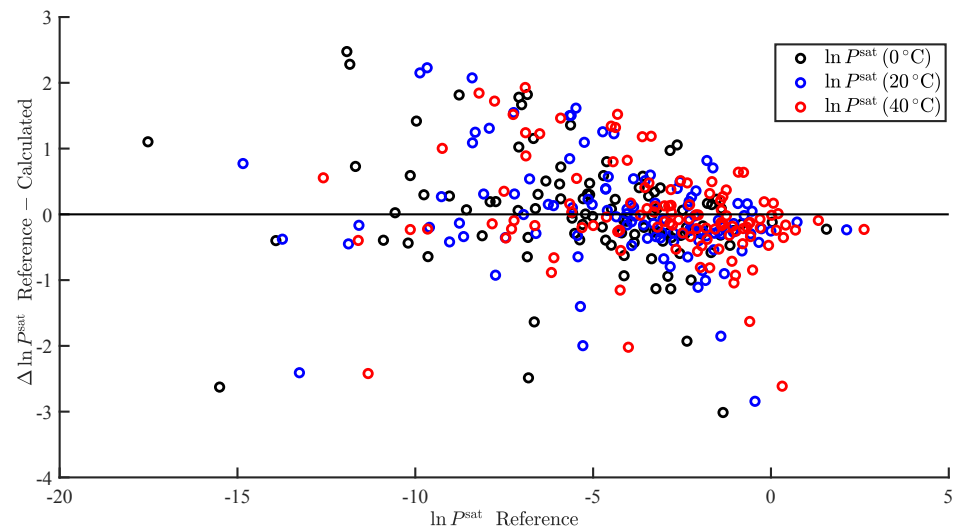


Figure 2. Residual plot of the difference between the reference and calculated (using Equation (17)) values of $\ln P^{\text{sat}}$ at 0, 20, and 40 °C, as indicated, versus the reference values. P^{sat} is in units of bar. The solid line corresponds to the $y = 0$ line and is drawn as a reference.

The ability of Equation (14) to correlate $\Delta H^{\text{vap}}/(RT)$ is illustrated in Figures 3 and 4, a parity and residual plot, respectively. In Figure 3, we likewise see that the values of $\Delta H^{\text{vap}}/(RT)$ were well correlated. In Figure 4, the error appears random. However, it did appear that the larger the value of $\Delta H^{\text{vap}}/(RT)$, the larger the deviation between the calculated and reference value was. As noted earlier, the effect of intermolecular interactions was to increase the value of $\Delta H^{\text{vap}}/(RT)$ as compared to the reference value. Therefore, the larger the deviation from the reference value, the larger the observed error was. This was exactly the same as found for $\ln P^{\text{sat}}$.

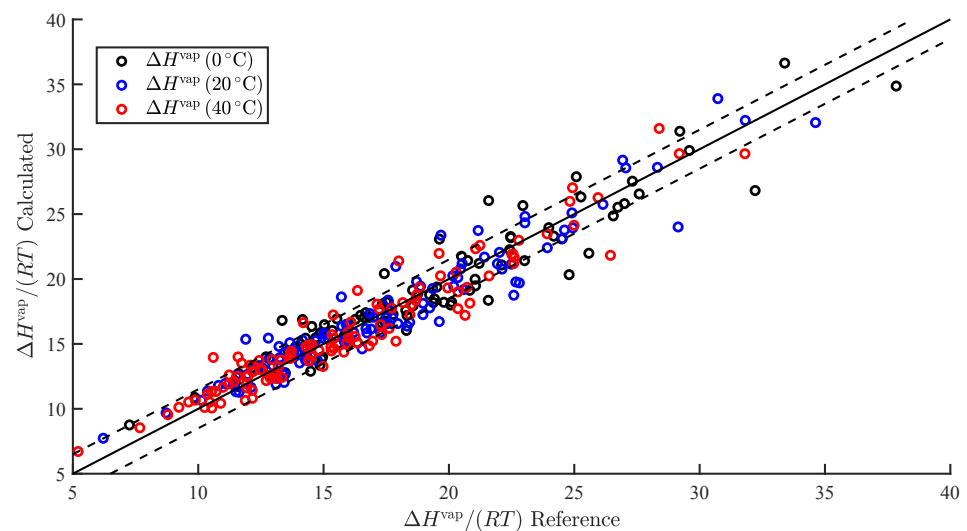


Figure 3. Parity plot of the dimensionless $\Delta H^{\text{vap}}/(RT)$ calculated using Equation (14) at 0, 20, and 40 °C, as indicated, versus the reference values. The solid line corresponds to the $y = x$ line, and the dashed lines correspond to plus or minus the root-mean-squared error (RMS) at 20 °C and are drawn as a reference.

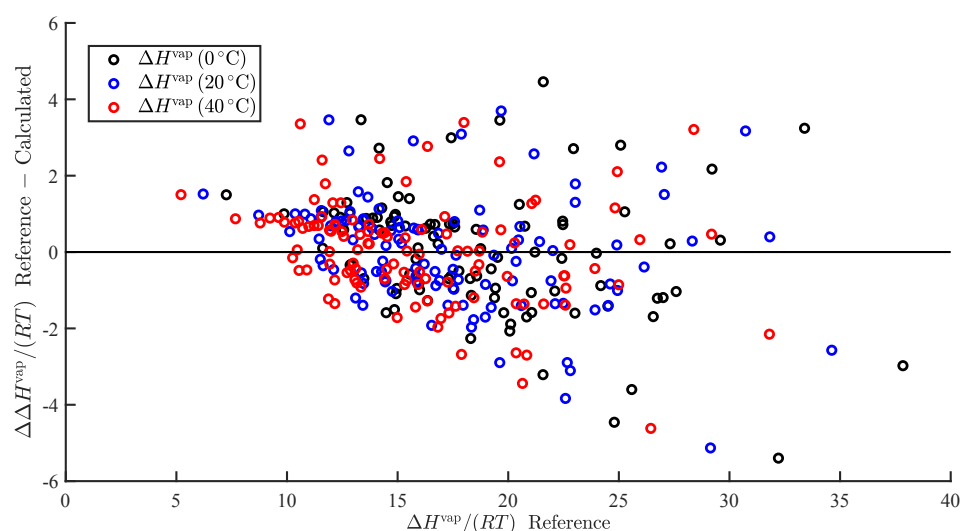


Figure 4. Residual plot of the difference between the reference and calculated (using Equation (14)) values of the dimensionless $\Delta H^{\text{vap}}/(RT)$ at 0, 20, and 40 °C, as indicated, versus the reference values. The solid line corresponds to the $y = 0$ line and is drawn as a reference.

3.2. Temperature-Dependent P^{sat}

Having correlated $\ln P^{\text{sat}}$ at 0, 20, and 40 °C, we next sought to use these values to obtain Antoine constants (see Equation (18)), which would allow one to interpolate and extrapolate to other temperatures. For the 130 organic solvents and water for which MOSCED parameters exist, we used the correlations to predict $\ln P^{\text{sat}}$ at 0, 20, and 40 °C. These values were then used to solve for the Antoine constants A , B , and C .

Unfortunately, this approach was not successful for phenol, *m*-cresol, acetic acid, and water. As temperature increases, P^{sat} increases and is equal to the critical pressure at the critical point. The issue was that our correlations at 0, 20, and 40 °C were independently correlated, and this requirement was, therefore, not enforced.

Given this limitation, we alternatively employed the Clausius–Clapeyron equation of the form [53]:

$$\ln P^{\text{sat}} = \ln P^{\text{sat},0} - \frac{\Delta H^{\text{vap},0}}{R} \frac{1}{T} \quad (21)$$

where P^{sat} is the vapor pressure at the temperature of interest, T , and $P^{\text{sat},0}$ and $\Delta H^{\text{vap},0}$ are the vapor pressure and enthalpy of vaporization at the reference temperature, T^0 . Within this expression, we assumed that the change in compressibility upon vaporization was approximately 1, $\Delta Z^{\text{vap}} \approx 1$, and the enthalpy of vaporization was constant and equal to the value at T^0 . Since $P^{\text{sat},0}$ and $\Delta H^{\text{vap},0}$ are constants and $\Delta H^{\text{vap},0} > 0$, Equation (21) ensures that as T increases, P^{sat} will increase.

Our assessment of the use of the Clausius–Clapeyron equation is provided in Table 3. Let us walk through the table so that we can better understand the result. In the first two columns, we indicate the temperature and the number of reference values of $\ln P^{\text{sat}}$ available at this temperature. In Columns 3 to 5, we report the standard deviation of the difference between the predicted and reference values (σ), AAPE, and RMS error for the correlation (Equation (17)) at the indicated temperature to quantify the goodness of fit. This information is the same as reported in Table 2, where we additionally included σ . We took the results of the correlation as a measure of the best we can hope to achieve at that temperature. Next, we made two sets of predictions using the Clausius–Clapeyron equation. In Column 6, we report the reference temperature used, and Columns 7 to 9 report the goodness of fit.

Table 3. Summary of the goodness of fit of using the correlation (Equation (17)) for $\ln P^{\text{sat}}$ at the temperature of interest as compared to the Clausius–Clapeyron equation (Equation (21)) with the indicated reference temperature. The goodness of fit is quantified using the standard deviation (σ), the average absolute percent error (AAPE), and the root-mean-squared error (RMS), where N corresponds to the number of organic compounds for which reference value of $\ln P^{\text{sat}}$ are available at the temperature of interest. The goodness of fit is computed for $\ln P^{\text{sat}}$, where P^{sat} is in units of bar.

T (°C)	N	σ	Correlation		Clausius–Clapeyron			
			AAPE (%)	RMS	T^0 (°C)	σ	AAPE (%)	RMS
0	102	0.64	18.25	0.87	20	0.70	70.80	0.90
					40	0.64	42.40	0.83
20	114	0.58	99.75	0.79	0	0.64	18.68	0.88
					40	0.54	41.86	0.74
40	117	0.54	40.10	0.74	0	0.67	14.55	0.88
					20	0.79	337.73	1.48

Consider the case of 0 °C. At 0 °C, reference values of $\ln P^{\text{sat}}$ were available for 102 compounds with the results of the correlation reported. For these 102 compounds, we then used Equations (17) and (14) to predict $\ln P^{\text{sat},0}$ and $\Delta H^{\text{vap},0}$ at the reference temperature (20 or 40 °C), as indicated. These reference values were then used in the Clausius–Clapeyron equation to predict $\ln P^{\text{sat}}$ at the temperature of interest, here 0 °C. These predicted values were then compared to the reference values of $\ln P^{\text{sat}}$.

While we did not expect the predictions using the Clausius–Clapeyron equation to be as accurate as the direct correlation at that temperature, we found that they did appear reasonable. We subsequently evaluated their accuracy for phase equilibria predictions by next predicting the values of $\mathcal{H}_{2,1}$ and $\Delta G_{2,1}^{\text{sol},v}$ in water.

3.3. $\mathcal{H}_{2,1}$ and $\Delta G_{2,1}^{\text{sol},v}$ in Water

To assess the use of the Clausius–Clapeyron equation (CC) to predict $\ln P^{\text{sat}}$ for phase equilibria calculation, we next predicted the log Henry’s constant ($\ln \mathcal{H}_{2,1}$, Equation (3)) and the solvation free energy ($\Delta G_{2,1}^{\text{sol},v}$, Equation (4)) for organic solutes (2) in water (1). The results are summarized in Tables 4 and 5. To assess the use of the CC for phase equilibria predictions, a comparison was made to the use of MOSCED with reference vapor pressures and the use of mod-UNIFAC to predict $\ln \gamma_2^\infty$ with reference vapor pressure values [54–59]; the data for this comparison were taken from our previous work [24].

Table 4. Summary of the error in the predicted log Henry’s constant ($\ln \mathcal{H}_{2,1}$, Equation (3)) for organic solutes in water, where $\mathcal{H}_{2,1}$ is in units of bar. The error is quantified using the standard deviation computed for the difference between the calculated and reference value (σ) and the root-mean-squared error (RMS), the average absolute percent error (AAPE), the average absolute error (AAE), and R^2 , where N is the number of organic solutes for which reference data were available. The majority of the data were at 25 °C. Predictions were made for MOSCED with $\ln P_2^{\text{sat}}$ computed using the Clausius–Clapeyron equation with a reference temperature of 20 and 40 °C, as indicated, plus the use of the reference vapor pressure for comparison. Predictions were additionally made using mod-UNIFAC with the reference vapor pressures.

P_2^{sat} Calc	σ	RMS	AAPE (%)	AAE	R^2	N
CC (20 °C)	1.08	1.20	64.72	0.94	0.96	81
CC (40 °C)	1.10	1.20	68.98	0.94	0.96	81
reference	0.97	1.07	10.61	0.74	0.97	81
mod-UNIFAC	2.12	3.73	27.77	3.08	0.63	60

Table 5. Summary of the error in the predicted solvation free energy ($\Delta G_{2,1}^{\text{solv}}$, Equation (4)) for organic solutes in water, where $\Delta G_{2,1}^{\text{solv}}$ is in units of kJ/mol. The error is quantified using the standard deviation computed for the difference between the calculated and reference value (σ) and the root-mean-squared error (RMS), the average absolute percent error (AAPE), the average absolute error (AAE), and R^2 , where N is the number of organic solutes for which reference data were available. All of the data were at 25 °C. Predictions were made for MOSCED with $\ln P_2^{\text{sat}}$ computed using the Clausius–Clapeyron equation with a reference temperature of 20 °C plus the use of the reference vapor pressure for comparison. Predictions were additionally made using mod-UNIFAC with the reference vapor pressures.

P_2^{sat} Calc	σ	RMS	AAPE (%)	AAE	R^2	N
CC (20 °C)	2.54	2.71	22.07	2.18	0.96	73
reference	2.52	2.73	22.89	2.04	0.96	73
mod-UNIFAC	4.88	9.31	229.80	7.95	0.70	60

For the case of $\ln \mathcal{H}_{2,1}$, we found that, with the use of the CC, all of the errors increase with respect to the use of the reference vapor pressure values. Nonetheless, the predictions remained very well correlated. Moreover, the predictions remained superior to the use of mod-UNIFAC. We note that the AAPE was smaller with mod-UNIFAC. However, the value of the AAPE is sensitive to deviations when the property of interest is close to zero. A residual plot for $\ln \mathcal{H}_{2,1}$ predicted using the CC is provided in Figure 5. The errors appeared random, suggesting there were no systematic errors in the predictions.

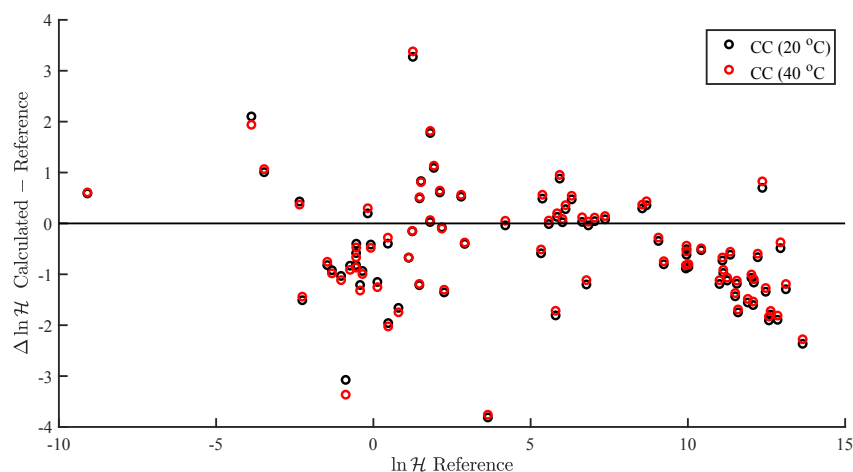


Figure 5. Residual plot of the difference between the reference and calculated log Henry's constant ($\ln \mathcal{H}_{2,1}$, Equation (3)) for organic solutes in water, versus the reference values. $\mathcal{H}_{2,1}$ is in units of bar. The solid line corresponds to the $y = 0$ line and is drawn as a reference. Predictions were made for MOSCED with $\ln P_2^{\text{sat}}$ computed using the Clausius–Clapeyron equation with a reference temperature of 20 and 40 °C, as indicated.

The results were similar for $\Delta G_{2,1}^{\text{solv}}$. Here, all of the reference data were a 25 °C, so we used only the CC with a reference temperature of 20 °C. Interestingly, the difference between the use of the CC and the reference values of $\ln P_2^{\text{sat}}$ was very small. Additionally, we again found that the MOSCED-based predictions were superior to the use of mod-UNIFAC. A residual plot for $\Delta G_{2,1}^{\text{solv}}$ predicted using the CC is provided in Figure 6. The errors appeared random, suggesting there were no systematic errors in the predictions.

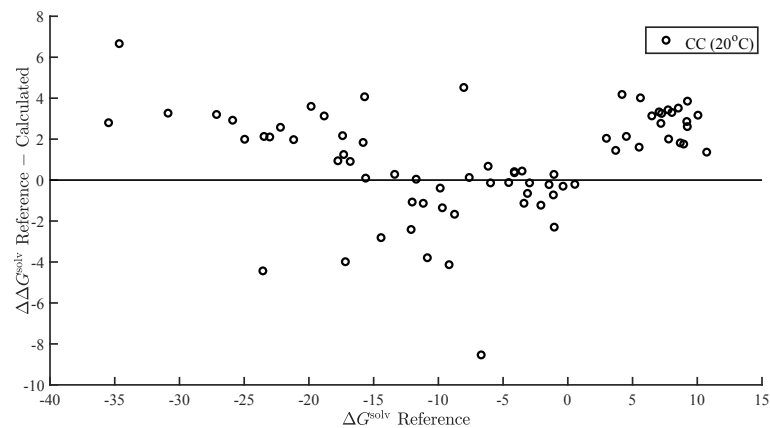


Figure 6. Residual plot of the difference between the reference and calculated solvation free energy ($\Delta G_{2,1}^{\text{solv}}$, Equation (4)) for organic solutes in water, versus the reference values. $\Delta G_{2,1}^{\text{solv}}$ is in units of kJ/mol. The solid line corresponds to the $y = 0$ line and is drawn as a reference. Predictions were made for MOSCED with $\ln P_2^{\text{sat}}$ computed using the Clausius–Clapeyron equation with a reference temperature of 20 °C.

3.4. Other Correlations

Finally, given the success in correlating $\ln P_2^{\text{sat}}$ and ΔH^{vap} using multiple linear regression, we attempted to correlate a range of additional properties. For surface tension (γ), this led to

$$\ln \gamma = a_0 + \frac{v^{1/3}}{RT} (a_1 \lambda^2 + a_2 \tau^2 + a_3 \alpha \beta + a_4 \alpha \alpha + a_5 \beta \beta) \quad (22)$$

for (dynamic) viscosity (μ):

$$\ln \mu = a_0 + \frac{v}{RT} (a_1 \lambda^2 + a_2 \tau^2 + a_3 \alpha \beta + a_4 \alpha \alpha + a_5 \beta \beta) \quad (23)$$

the normal melting point (T_m):

$$T_m = a_0 + \frac{v^{1/2}}{R} (a_1 \lambda^2 + a_2 \tau^2 + a_3 \alpha \beta + a_4 \alpha \alpha + a_5 \beta \beta) \quad (24)$$

the normal boiling point (T_b):

$$T_b = a_0 + \frac{v}{R} (a_1 \lambda^2 + a_2 \tau^2 + a_3 \alpha \beta + a_4 \alpha \alpha + a_5 \beta \beta) \quad (25)$$

the acentric factor (ω):

$$\omega = a_0 + \frac{v}{R} (a_1 \lambda^2 + a_2 \tau^2 + a_3 \alpha \beta + a_4 \alpha \alpha + a_5 \beta \beta) \quad (26)$$

the normal enthalpy of fusion (ΔH^{fus}):

$$\frac{\Delta H^{\text{fus}}}{R} = a_0 + \frac{v}{R} (a_1 \lambda^2 + a_2 \tau^2 + a_3 \alpha \beta + a_4 \alpha \alpha + a_5 \beta \beta) \quad (27)$$

the critical pressure (P_c):

$$\ln P_c = a_0 + \frac{v}{R} (a_1 \lambda^2 + a_2 \tau^2 + a_3 \alpha \beta + a_4 \alpha \alpha + a_5 \beta \beta) \quad (28)$$

and the critical temperature (T_c):

$$T_c = a_0 + \frac{v^{1/2}}{R} (a_1 \lambda^2 + a_2 \tau^2 + a_3 \alpha \beta + a_4 \alpha \alpha + a_5 \beta \beta) \quad (29)$$

In general, we eliminated T in the right-hand-side of the equation when the temperature of the property was not the same for each compound, and we manually varied the power of v in an attempt to improve the fit for $\ln \gamma$ and T_c . We note that the scaling of $v^{1/3}$ used here for $\ln \gamma$ was also used by Koenhen and Smolders [60] for γ . The results are provided in Table 6.

Table 6. Summary of the regressed model parameters using Equations (22)–(29) along with the Pearson correlation coefficient (R^2), the root-mean-squared error (RMS), and the average absolute percent error (AAPE) to assess the goodness of fit, where N corresponds to the number of organic compounds included in the fit. In the correlations, γ is in units of dyn/cm, μ is in cP, T_m , T_b , and T_c are all in K, ω is dimensionless, $\Delta H^{\text{fus}}/R$ is in units of K, and P_c is in units of bar. When applicable, the temperature indicates the temperature at which the regression was performed.

Property	a_0	a_1	a_2	a_3	a_4	a_5	R^2	RMS	AAPE (%)	N
$\ln \gamma(0^\circ\text{C})$	−2.23	49.65	95.21	38.17	2.15	−1.23	0.82	3.28	3.03	96
$\ln \gamma(20^\circ\text{C})$	−4.72	54.03	102.96	45.08	−0.82	−2.92	0.82	3.31	9.07	112
$\ln \gamma(40^\circ\text{C})$	−6.82	57.61	105.70	45.82	−0.63	−2.36	0.84	3.18	9.56	118
$\ln \mu(0^\circ\text{C})$	−2.65	0.15	0.51	0.62	0.05	−0.03	0.81	0.42	204.22	77
$\ln \mu(20^\circ\text{C})$	−2.40	0.13	0.41	0.64	−0.03	−0.01	0.79	0.43	342.72	112
$\ln \mu(40^\circ\text{C})$	−0.49	0.25	0.77	1.05	0.06	0.00	0.80	6.51	96.06	117
T_m	33.80	0.45	0.65	0.40	0.06	0.02	0.56	35.27	13.95	124
T_b	214.45	0.04	0.11	0.08	0.00	0.00	0.88	24.00	4.33	127
ω	0.06	0.00	0.00	0.00	0.00	0.00	0.61	0.09	19.98	122
$\Delta H^{\text{fus}}/R$	−792.98	0.55	0.42	0.55	−0.09	0.00	0.56	603.18	86.51	114
$\ln P_c$	4.21	−0.05	0.02	0.01	0.01	0.00	0.64	0.19	4.21	121
T_c	220.99	0.97	1.44	0.82	0.01	0.02	0.85	33.86	7.91	121

Unfortunately, these predictions are inferior to those for $\ln P^{\text{sat}}$ and ΔH^{vap} . Further efforts are necessary to improve their predictive abilities. The results are nonetheless interesting. Consider the case of surface tension; the correlations suggested that dispersion, polar, and self-association interactions increased the observed surface tension.

4. Summary and Conclusions

In the present study, we demonstrated and assessed the ability of MOSCED to correlate the enthalpy of vaporization and vapor pressure at a specific temperature using multiple linear regression. MOSCED is a solubility-parameter-based method, wherein the parameters correspond to specific, physical intermolecular interactions. In this way, MOSCED can be used to both predict phase equilibria and shed light on the underlying intermolecular interactions, which is advantageous for early-stage process development and design.

MOSCED is based on the theory that the cohesive energy may be separated into individual contributions (due to specific intermolecular interactions), which are additive. The cohesive energy is directly related to the enthalpy of vaporization, and MOSCED has, in turn, been shown previously to well correlate the enthalpy of vaporization. Here, we showed that MOSCED is additionally able to correlate the log vapor pressure. While MOSCED can be used to predict limiting activity coefficients, the additional ability to predict vapor pressure extends MOSCED to be able to predict vapor–liquid phase equilibrium devoid of reference data. Here, this was demonstrated by using MOSCED to predict the Henry’s constant and solvation free energy of organic solutes in water. While the errors in the predicted Henry’s constant were slightly larger when MOSCED was used to additionally predict the vapor pressure, the difference was small and still superior to the use of mod-UNIFAC. The same was true with the solvation free energy; only the difference between the use of reference and MOSCED predicted vapor pressures was insignificant. In the most-recent MOSCED revision, parameters were regressed for 130 organic com-

pounds. This was limited due to the availability of reference limiting activity coefficients. In addition to being able to make phase equilibrium predictions, the ability to correlate the enthalpy of vaporization and vapor pressure offers the opportunity to include additional properties in the regression of MOSCED parameters.

Given the success in correlating the enthalpy of vaporization and vapor pressure, we attempted to correlate a wide range of physical properties using similar expressions. While, in some cases, the results were reasonable, they were inferior to the correlations of the enthalpy of vaporization and vapor pressure. Future efforts will be needed to improve the correlations.

Supplementary Materials: The following supporting information can be downloaded at: <https://www.mdpi.com/article/10.3390/chemengineering7020025/s1>.

Author Contributions: Conceptualization, P.D. and A.S.P.; data curation, S.N.R.; formal analysis, N.H.W.; funding acquisition, A.S.P.; methodology, P.D., N.H.W. and A.S.P.; project administration, A.S.P.; software, N.H.W.; supervision, A.S.P.; validation, N.H.W. and A.S.P.; visualization, N.H.W.; writing—original draft, N.H.W. and A.S.P.; writing—review and editing, N.H.W. and A.S.P. All authors have read and agreed to the published version of the manuscript.

Funding: This research received no external funding.

Data Availability Statement: The reference pure component properties were sourced from *Yaws' Handbook of Thermodynamic and Physical Properties of Chemical Compounds* [45]. The compiled reference data and MOSCED parameters are provided in the Supporting Information accompanying the electronic version of this manuscript. We additionally provide MATLAB code used to perform the multiple linear regression for ΔH^{vap} and $\ln P^{\text{sat}}$ at 0, 20, and 40 °C.

Conflicts of Interest: The authors declare no conflict of interest.

References

1. Wankat, P.C. *Separation Process Engineering: Includes Mass Transfer*, 3rd ed.; Pearson Education, Inc.: Upper Saddle River, NJ, USA, 2012.
2. Gmehling, J.; Menke, J.; Krafczyk, J.; Fischer, K. *Azeotropic Data, Part 1*, 2nd ed.; WILEY-VCH Verlag GmbH & Co. KGaA: Weinheim, Germany, 2004.
3. *Materials for Separation Technologies: Energy and Emission Reduction Opportunities*; Technical Report; U.S. Department of Energy: Washington, DC, USA, 2005.
4. Prausnitz, J.M.; Lichtenthaler, R.N.; de Azevedo, E.G. *Molecular Thermodynamics of Fluid-phase Equilibria*, 2nd ed.; Prentice-Hall, Inc.: Englewood Cliffs, NJ, USA, 1986.
5. Hildebrand, J.H.; Prausnitz, J.M.; Scott, R.L. *Regular and Related Solutions*; Van Nostrand Reinhold Company: New York, NY, USA, 1970.
6. Hansen, C.M. The Universality of the Solubility Parameter. *Ind. Eng. Chem. Prod. Res. Dev.* **1969**, *8*, 2–11. [[CrossRef](#)]
7. Panayiotou, C. Redefining solubility parameters: The partial solvation parameters. *Phys. Chem. Chem. Phys.* **2012**, *14*, 3882–3908. [[CrossRef](#)] [[PubMed](#)]
8. Stefanis, E.; Panayiotou, C. A new expanded solubility parameter approach. *Int. J. Pharm.* **2012**, *426*, 29–43. [[CrossRef](#)] [[PubMed](#)]
9. Beerbower, A.; Wu, P.L.; Martin, A. Expanded Solubility Parameter Approach I: Naphthalene and Benzoic Acid in Individual Solvents. *J. Pharm. Sci.* **1984**, *73*, 179–188. [[CrossRef](#)] [[PubMed](#)]
10. Louwerse, M.J.; Maldonado, A.; Rousseau, S.; Moreau-Masselon, C.; Roux, B.; Rothenberg, G. Revisiting Hansen Solubility Parameters by Including Thermodynamics. *ChemPhysChem* **2017**, *18*, 2999–3006. [[CrossRef](#)]
11. Blanks, R.F.; Prausnitz, J.M. Thermodynamics of Polymer Solubility in Polar and Nonpolar Systems. *Ind. Eng. Chem. Fundam.* **1964**, *3*, 1–8. [[CrossRef](#)]
12. Tijssen, R.; Billiet, H.A.H.; Schoenmakers, P.J. Use of the solubility parameter for predicting selectivity and retention in chromatography. *J. Chromatogr. A* **1976**, *122*, 185–203. [[CrossRef](#)]
13. Krooshof, G.J.P.; Tuinier, R.; de With, G. Generalization of Guggenheim's combinatorial activity coefficient equation. *J. Mol. Liq.* **2018**, *266*, 467–471. [[CrossRef](#)]
14. Krooshof, G.J.P.; Tuinier, R.; de With, G. On the calculation of nearest neighbors in activity coefficient models. *Fluid Phase Equilib.* **2018**, *465*, 10–23. [[CrossRef](#)]
15. Thomas, E.R.; Eckert, C.A. Prediction of limiting activity coefficients by a modified separation of cohesive energy density model and UNIFAC. *Ind. Eng. Chem. Proc. Des. Dev.* **1984**, *23*, 194–209. [[CrossRef](#)]
16. Park, J.H.; Carr, P.W. Predictive Ability of the MOSCED and UNIFAC Activity Coefficient Estimation Methods. *Anal. Chem.* **1987**, *59*, 2596–2602. [[CrossRef](#)]

17. Howell, W.J.; Karachewski, A.M.; Stephenson, K.M.; Eckert, C.A.; Park, J.H.; Carr, P.W.; Rutan, S.C. An Improved MOSCED Equation for the Prediction and Application of Infinite Dilution Activity Coefficients. *Fluid Phase Equilib.* **1989**, *52*, 151–160. [[CrossRef](#)]
18. Hait, M.J.; Liotta, C.L.; Eckert, C.A.; Bergmann, D.L.; Karachewski, A.M.; Dallas, A.J.; Eikens, D.I.; Li, J.J.; Carr, P.W.; Poe, R.B.; et al. Space Predictor for Infinite Dilution Activity Coefficients. *Ind. Eng. Chem. Res.* **1993**, *32*, 2905–2914. [[CrossRef](#)]
19. Castells, C.B.; Carr, P.W.; Eikens, D.I.; Bush, D.; Eckert, C.A. Comparative Study of Semitheoretical Models for Predicting Infinite Dilution Activity Coefficients of Alkanes in Organic Solvents. *Ind. Eng. Chem. Res.* **1999**, *38*, 4104–4109. [[CrossRef](#)]
20. Lazzaroni, M.J.; Bush, D.; Eckert, C.A.; Frank, T.C.; Gupta, S.; Olson, J.D. Revision of MOSCED Parameters and Extension to Solid Solubility Calculations. *Ind. Eng. Chem. Res.* **2005**, *44*, 4075–4083. [[CrossRef](#)]
21. Draucker, L.C.; Janakat, M.; Lazzaroni, M.J.; Bush, D.; Eckert, C.A.; Frank, T.C.; Olson, J.D. Experimental determination and model prediction of solid solubility of multifunctional compounds in pure and mixed nonelectrolyte solvents. *Ind. Eng. Chem. Res.* **2007**, *46*, 2198–2204. [[CrossRef](#)]
22. Frank, T.C.; Anderson, J.J.; Olson, J.D.; Eckert, C.A. Application of MOSCED and UNIFAC to screen hydrophobic solvents for extraction of hydrogen-bonding organics from aqueous solution. *Ind. Eng. Chem. Res.* **2007**, *46*, 4621–4625. [[CrossRef](#)]
23. Widenski, D.J.; Abbas, A.; Romagnoli, J.A. Use of Predictive Solubility Models for Isothermal Antisolvent Crystallization Modeling and Optimization. *Ind. Eng. Chem. Res.* **2011**, *50*, 8304–8313. [[CrossRef](#)]
24. Dhakal, P.; Roese, S.N.; Stalcup, E.M.; Paluch, A.S. Application of MOSCED to Predict Hydration Free Energies, Henry's Constants, Octanol/Water Partition Coefficients, and Isobaric Azeotropic Vapor-Liquid Equilibrium. *J. Chem. Eng. Data* **2018**, *63*, 352–364. [[CrossRef](#)]
25. Eckert, C.A.; Newman, B.A.; Nicolaidis, G.L.; Long, T.C. Measurement and Application of Limiting Activity Coefficients. *AIChE J.* **1981**, *27*, 33–40. [[CrossRef](#)]
26. Missen, R.W. On Criteria for Occurrence of Azeotropes in Isothermal and Isobaric Binary Systems. *Can. J. Chem. Eng.* **2005**, *83*, 667–674. [[CrossRef](#)]
27. Brandani, V. Use of Infinite-Dilution Activity Coefficients for Predicting Azeotrope Formation at Constant Temperature and Partial Miscibility in Binary Liquid Mixtures. *Ind. Eng. Chem. Fundam.* **1974**, *13*, 154–156. [[CrossRef](#)]
28. Schreiber, L.B.; Eckert, C.A. Use of Infinite Dilution Activity Coefficients with Wilson's Equation. *Ind. Eng. Chem. Process Des. Develop.* **1971**, *10*, 572–576. [[CrossRef](#)]
29. Dhakal, P.; Roese, S.N.; Stalcup, E.M.; Paluch, A.S. GC-MOSCED: A Group Contribution Method for Predicting MOSCED Parameters with Application to Limiting Activity Coefficients in Water and Octanol/Water Partition Coefficients. *Fluid Phase Equilib.* **2018**, *470*, 232–240. [[CrossRef](#)]
30. Gnap, M.; Elliott, J.R. Estimation of MOSCED parameters from the COSMO-SAC database. *Fluid Phase Equilib.* **2018**, *470*, 241–248. [[CrossRef](#)]
31. Churchill, B.; Acree, Jr., W.E.; Abraham, M.H. Development of Abraham model expressions for predicting the standard molar enthalpies of vaporization of organic compounds at 298.15 K. *Thermochim. Acta* **2019**, *681*, 178372. [[CrossRef](#)]
32. Quina, F.H.; Carroll, F.A.; Cheuy, D.H. A Linear Solvation Energy Relationship to Predict Vapor Pressure from Molecular Structure. *J. Braz. Chem. Soc.* **2005**, *16*, 1010–1016. [[CrossRef](#)]
33. Vitha, M.; Carr, P.W. The chemical interpretation and practice of linear solvation energy relationships in chromatography. *J. Chromatogr. A* **2006**, *1126*, 143–194. [[CrossRef](#)]
34. Dhakal, P.; Ouimet, J.A.; Roese, S.N.; Paluch, A.S. MOSCED parameters for 1-n-alkyl-3-methylimidazolium-based ionic liquids: Application to limiting activity coefficients and intuitive entrainer selection for extractive distillation processes. *J. Mol. Liq.* **2019**, *293*, 111552. [[CrossRef](#)]
35. Dhakal, P.; Weise, A.R.; Fritsch, M.C.; O'Dell, C.M.; Paluch, A.S. Expanding the Solubility Parameter Method MOSCED to Pyridinium, Quinolinium, Pyrrolidinium, Piperidinium, Bicyclic, Morpholinium, Ammonium, Phosphonium, and Sulfonium Based Ionic Liquids. *ACS Omega* **2020**, *5*, 3863–3877. [[CrossRef](#)]
36. Dhakal, P.; Roese, S.N.; Lucas, M.A.; Paluch, A.S. Predicting Limiting Activity Coefficients and Phase Behavior from Molecular Structure: Expanding MOSCED to Alkanediols Using Group Contribution Methods and Electronic Structure Calculations. *J. Chem. Eng. Data* **2018**, *63*, 2586–2598. [[CrossRef](#)]
37. Ley, R.T.; Fuerst, G.B.; Redeker, B.N.; Paluch, A.S. Developing a Predictive Form of MOSCED for Nonelectrolyte Solids Using Molecular Simulation: Application to Acetanilide, Acetaminophen, and Phenacetin. *Ind. Eng. Chem. Res.* **2016**, *55*, 5415–5430. [[CrossRef](#)]
38. Phifer, J.R.; Solomon, K.J.; Young, K.L.; Paluch, A.S. Computing MOSCED parameters of nonelectrolyte solids with electronic structure methods in SMD and SM8 continuum solvents. *AIChE J.* **2017**, *63*, 781–791. [[CrossRef](#)]
39. Phifer, J.R.; Cox, C.E.; da Silva, L.F.; Nogueira, G.G.; Barbosa, A.K.P.; Ley, R.T.; Bozada, S.M.; O'Loughlin, E.J.; Paluch, A.S. Predicting the equilibrium solubility of solid polycyclic aromatic hydrocarbons and dibenzothiophene using a combination of MOSCED plus molecular simulation or electronic structure calculations. *Mol. Phys.* **2017**, *115*, 1286–1300. [[CrossRef](#)]
40. Marrero, J.; Gani, R. Group-contribution based estimation of pure component properties. *Fluid Phase Equilib.* **2001**, *183–184*, 183–208. [[CrossRef](#)]
41. Hukkerikar, A.S.; Sarup, B.; Kate, A.T.; Abildskov, J.; Sin, G.; Gani, R. Group-contribution+ (GC+) based estimation of properties of pure components: Improved property estimation and uncertainty analysis. *Fluid Phase Equilib.* **2012**, *321*, 25–43. [[CrossRef](#)]

42. Gharagheizi, F.; Eslamimanesh, A.; Ilani-Kashkouli, P.; Mohammadi, A.H.; Richon, D. Determination of Vapor Pressure of Chemical Compounds: A Group Contribution Model for an Extremely Large Database. *Ind. Eng. Chem. Res.* **2012**, *51*, 7119–7125. [[CrossRef](#)]
43. Poe, R.B.; Rutan, S.C.; Hait, M.J.; Eckert, C.A.; Carr, P.W. Developing Models for Infinite Dilution Activity-Coefficients Using Factor-Analysis Methods. *Anal. Chim. Acta* **1993**, *277*, 223–238. [[CrossRef](#)]
44. Watson, K.M. Thermodynamics of the Liquid State. *Ind. Eng. Chem.* **1943**, *35*, 398–406. [[CrossRef](#)]
45. Yaws, C.L. *Yaws' Handbook of Thermodynamic and Physical Properties of Chemical Compounds*; Knovel: New York, NY, USA 2003; ISBN: 978-1-59124-444-8.
46. Verevkin, S.P. Measurement and Prediction of the Monocarboxylic Acids Thermochemical Properties. *J. Chem. Eng. Data* **2000**, *45*, 953–960. [[CrossRef](#)]
47. MATLAB. *R2019a*; The MathWorks Inc.: Natick, MA, USA, 2019.
48. Lay, D.C. *Linear Algebra and Its Applications*, 3rd ed.; Addison Wesley, Inc.: Boston, MA, USA, 2003.
49. Yaws, C.L. *Yaws' Handbook of Properties for Aqueous Systems*; Knovel: New York, NY, USA 2012; ISBN: 978-1-62198-034-6.
50. Mobley, D.L.; Guthrie, J.P. FreeSolv: A database of experimental and calculated hydration free energies, with input files. *J. Comput.-Aided Mol. Des.* **2014**, *28*, 711–720. [[CrossRef](#)] [[PubMed](#)]
51. Matos, G.D.R.; Kyu, D.Y.; Loeffler, H.H.; Chodera, J.D.; Shirts, M.R.; Mobley, D.L. Approaches for Calculating Solvation Free Energies and Enthalpies Demonstrated with an Update of the FreeSolv Database. *J. Chem. Eng. Data* **2017**, *62*, 1559–1569. [[CrossRef](#)] [[PubMed](#)]
52. FreeSolv: Experimental and Calculated Small Molecule Hydration Free Energies, Version 0.51. Available online: <https://github.com/MobleyLab/FreeSolv> (accessed on 11 June 2017).
53. Poling, B.E.; Prausnitz, J.M.; O'Connell, J.P. *The Properties of Gases and Liquids*, 5th ed.; The McGraw-Hill Companies, Inc.: New York, NJ, USA, 2001.
54. Weidlich, U.; Gmehling, J. A Modified UNIFAC Model. 1. Prediction of VLE, h^E , and γ^∞ . *Ind. Eng. Chem. Res.* **1987**, *26*, 1372–1381. [[CrossRef](#)]
55. Gmehling, J.; Li, J.; Schiller, M. A Modified UNIFAC Model. 2. Present Parameter Matrix and Results for Different Thermodynamic Properties. *Ind. Eng. Chem. Res.* **1993**, *32*, 178–193. [[CrossRef](#)]
56. Gmehling, J.; Lohmann, J.; Jakob, A.; Li, J.; Joh, R. A Modified UNIFAC (Dortmund) Model. 3. Revision and Extension. *Ind. Eng. Chem. Res.* **1998**, *37*, 4876–4882. [[CrossRef](#)]
57. Gmehling, J.; Wittig, R.; Lohmann, J.; Joh, R. A Modified UNIFAC (Dortmund) Model. 4. Revision and Extension. *Ind. Eng. Chem. Res.* **2002**, *41*, 1678–1688. [[CrossRef](#)]
58. Jakob, A.; Grensemann, H.; Lohmann, J.; Gmehling, J. Further Development of Modified UNIFAC (Dortmund): Revision and Extension 5. *Ind. Eng. Chem. Res.* **2006**, *45*, 7924–7933. [[CrossRef](#)]
59. Constantinescu, D.; Gmehling, J. Further Development of Modified UNIFAC (Dortmund): Revision and Extension 6. *J. Chem. Eng. Data* **2016**, *61*, 2738–2748. [[CrossRef](#)]
60. Koenhen, D.M.; Smolders, C.M. The Determination of Solubility Parameters of Solvents and Polymers by Means of Correlations with Other Physical Quantities. *J. Appl. Polym. Sci.* **1975**, *19*, 1163–1179. [[CrossRef](#)]

Disclaimer/Publisher's Note: The statements, opinions and data contained in all publications are solely those of the individual author(s) and contributor(s) and not of MDPI and/or the editor(s). MDPI and/or the editor(s) disclaim responsibility for any injury to people or property resulting from any ideas, methods, instructions or products referred to in the content.